


RESEARCH

Open Access



# Circulating small extracellular vesicles microRNAs plus CA-125 for treatment stratification in advanced ovarian cancer

Xiaofang Zhou<sup>1,7†</sup>, Mu Liu<sup>1†</sup>, Lijuan Sun<sup>2</sup>, Yumei Cao<sup>2</sup>, Shanmei Tan<sup>3</sup>, Guangxia Luo<sup>3</sup>, Tingting Liu<sup>4</sup>, Ying Yao<sup>5</sup>, Wangli Xiao<sup>5</sup>, Ziqing Wan<sup>1</sup> and Jie Tang<sup>1,6\*</sup> 

## Abstract

**Background** No residual disease (R0 resection) after debulking surgery is the most critical independent prognostic factor for advanced ovarian cancer (AOC). There is an unmet clinical need for selecting primary or interval debulking surgery in AOC patients using existing prediction models.

**Methods** RNA sequencing of circulating small extracellular vesicles (sEVs) was used to discover the differential expression microRNAs (DEMs) profile between any residual disease (R0, n = 17) and no residual disease (non-R0, n = 20) in AOC patients. We further analyzed plasma samples of AOC patients collected before surgery or neoadjuvant chemotherapy via TaqMan qRT-PCR. The combined risk model of residual disease was developed by logistic regression analysis based on the discovery-validation sets.

**Results** Using a comprehensive plasma small extracellular vesicles (sEVs) microRNAs (miRNAs) profile in AOC, we identified and optimized a risk prediction model consisting of plasma sEVs-derived 4-miRNA and CA-125 with better performance in predicting R0 resection. Based on 360 clinical human samples, this model was constructed using least absolute shrinkage and selection operator (LASSO) and logistic regression analysis, and it has favorable calibration and discrimination ability (AUC:0.903; sensitivity:0.897; specificity:0.910; PPV:0.926; NPV:0.871). The quantitative evaluation of Net Reclassification Improvement (NRI) and Integrated Discrimination Improvement (IDI) suggested that the additional predictive power of the combined model was significantly improved contrasted with CA-125 or 4-miRNA alone (NRI = 0.471, IDI = 0.538,  $p < 0.001$ ; NRI = 0.122, IDI = 0.185,  $p < 0.01$ ).

**Conclusion** Overall, we established a reliable, non-invasive, and objective detection method composed of circulating tumor-derived sEVs 4-miRNA plus CA-125 to preoperatively anticipate the high-risk AOC patients of residual disease to optimize clinical therapy.

**Keywords** Ovarian cancer, Residual disease, Small extracellular vesicles, microRNA, Prediction model

<sup>†</sup>Xiaofang Zhou and Mu Liu have contributed to this paper equally.

\*Correspondence:

Jie Tang

tangjie@hnca.org.cn

Full list of author information is available at the end of the article



## Introduction

Approximately 75% of ovarian cancer cases are not detected until stage III-IV, leading to a 5 year survival rate of less than 30% [1]. Although the best timing for surgery has been controversial, no residual disease (R0 resection) following primary debulking surgery (PDS) is recognized as the most potent determinant of clinical prognosis in advanced ovarian cancer (AOC, high-grade serous ovarian cancer (HGSOC) with FIGO stage III or IV) [2, 3]. Two famous randomized clinical trials have confirmed that neoadjuvant chemotherapy followed by interval debulking surgery (NACT-IDS) has similar progression-free survival and overall survival with fewer surgical complications compared to PDS for AOC patients who cannot achieve R0 resection [4]. In this context, the preoperative identification of patients with unresectable tumors is of utmost importance to optimize the therapeutic choice between PDS and NACT. For commonly used clinical models, CA-125 has no accurate predictive threshold because the preoperative level cannot fully reflect the tumor progression [5, 6], and the radiological evaluation is subjective to some extent. Moreover, using the classic Fagotti laparoscopy scoring [7, 8] as a minimally invasive examination, with a 40.5% unsuccessful prediction operations rate, can lead to a delay in starting chemotherapy and may also facilitate tumor implantation metastasis in puncture sites [9].

At present, biomarkers of liquid biopsies to predict which AOC patients will potentially profit from PDS or NACT therapy are missing. Small extracellular vesicles (sEVs) are membrane vesicles with a diameter of less than 200 nm, which contain specific cargoes that represent selected portions of the source cell's contents, strongly biasing toward microRNAs (miRNAs) [10]. Mounting evidence suggests that sEVs-derived miRNAs could be used for cancer detection, and prognosis, and to guide therapy [11, 12]. Circulating concentrations of sEVs miRNAs vary in response to OC stages [13, 14], and their stability in stored samples makes them plausible candidates as biomarkers.

In this study, we assessed the diagnostic performance of circulating sEV-miRNAs plus CA-125 to distinguish high-risk AOC patients of residual disease for the purpose of treatment stratification into PDS or NACT-IDS.

## Materials and methods

### Clinical samples and ethics approval

A total of 221 AOC patients (HGSOC with FIGO stage III or IV) who were treated with PDS or NACT-IDS from January 2018 to June 2022 were recruited in this study (R0, n=99; non-R0, n=122). In addition, we obtained plasma samples from benign pelvic diseases (n=21), early-stage ovarian cancer with FIGO stage I

or II (n=20), and advanced colorectal cancer (n=22) patients. We also collected primary tumor tissues (n=58) and other site tissues (n=18) from these AOC patients after PDS. None of the patients involved had infectious diseases. AOC samples with the following characteristics were removed: (1) treatment with surgical operation or chemotherapy before plasma collection; (2) hemolysis. Each participant signed a written informed consent form. The study obtained ethical approval (No. KYJJ-2019-043) from the Hunan Cancer Hospital Institutional Review Board. The CA-125 level of each AOC patient was measured by chemiluminescence assay (Beckman, DXI800, CA, USA) before treatment at four clinical centers. Blood samples (8 mL) from every individual in a fasting state were collected with an EDTA-K2 anticoagulant tube in the early morning, stored at 4 °C, and then processed within 30 min. The samples were extracted via centrifugation at 2000×g for 10 min, and 13,000×g for 10 min at 4 °C to exclude effects from platelet-derived vesicles as described in refs. [15, 16]. Then the isolated plasma was aliquoted into 2 mL tubes for storage at - 80 °C. Samples from other centers were also processed as described above and then transported via dry ice.

### Isolation and purification of sEVs from plasma

sEVs were purified from 2 mL of plasma from AOC patients by differential ultracentrifugation [16]. After the plasma sample was thawed on ice, centrifuged at 3000×g for 15 min. The supernatant was carefully pipetted into a new tube and diluted with PBS to 23 mL, and centrifuged at 13,000×g for 30 min (Beckman Coulter, Brea, CA, USA). Through a 0.22 μm filter, the supernatant was ultracentrifuged at 100,000×g for 2 h at 4 °C to collect a pellet of sEVs. The pellet was dissolved with PBS, transferred to a new ultracentrifuge tube and centrifuged again at 100,000×g 4 °C for 2 h to eliminate any contaminants from the protein aggregates. Finally, the enriched pellet of sEVs was resuspended twice with 100 μL PBS and then collected into a new tube. The isolation method of plasma sEVs was performed strictly according to the MISEV2018 guidelines [17].

### Isolation and purification of sEVs from tissue

Primary tumor tissue, matched adjacent tissue, metastatic tumor tissue, and distant normal tissue were collected from AOC patients undergoing PDS. After collecting the living tissue, residual blood was washed with PBS, cut into 500 mg per block, and then placed in a frozen tube. The tissue was quickly transferred into liquid nitrogen flash-frozen for 1 h, and then stored at - 80 °C. Tissue sEVs were separated based on the protocol previously established by Vella et al. [18]. with some modifications [19]. Tissue dissociation was performed using

the Miltenyi Human Tumor Dissociation Kit (Miltenyi Biotec, No. 130-095-929, Germany). Before extraction, it was resuspended by enzymes H, R, and A, according to the instructions, and the dissociated mixture containing 2.2 mL RPMI, 100  $\mu$ L enzyme H, 50  $\mu$ L enzyme R, and 12.5  $\mu$ L enzyme A was prepared. A small piece of tissue (~200 mg) was weighed, and ultrathin sections were taken using a frozen slicer (to minimize foreign contamination caused by tissue cell rupturing, thereby enlarging the surface area). Then, the dissociation mixture prepared above was added and incubated at 37 °C for 15 min to enzymatic dissociation and permeabilize the tissue. Halt protease and phosphatase inhibitor single-use cocktail, EDTA-free (100X) (Thermo Scientific, No. 78443, USA) was added into dissociation solution and gently filtered twice through a 70  $\mu$ m filter to remove residual tissue.

The mixed suspension was centrifuged at 300 $\times$ g for 10 min at 4 °C. The supernatant was transferred to a new centrifuge tube and centrifuged at 2000 $\times$ g for 10 min at 4 °C. The cell-free supernatant was centrifuged at 10,000 $\times$ g for 20 min at 4 °C and then gently passed through a 0.22  $\mu$ m filter to remove remaining cell debris. The supernatant underwent additional ultracentrifugation at 150,000 $\times$ g for 2 h at 4 °C. The precipitates were collected and resuspended in 1 mL PBS, and further purified by an Exosupur column (Echobiotech, China). Finally, the sEVs-containing fraction was condensed to 200  $\mu$ L via a 100 kDa Amicon Ultra ultrafiltration centrifuge tube (Merck, Germany).

#### Separating sEVs by immunoaffinity magnetic bead sorting system (MACS)

Plasma and tissue sEVs were isolated via the above methods. Then, 20  $\mu$ L of magnetic microbeads with antibodies (EpCAM, FAP, CD31, CD235a, CD45; Miltenyi Biotec) was added to 100  $\mu$ L of sEVs suspension. After incubation for 60 min at 4 °C, the magnetic immune mixture was resuspended with 1 mL of PBS. The LD column (Miltenyi Biotec) was placed in a magnetic rack, and the column was washed three times with 2 mL PBS. The magnetic immune mixture was added to the LD column and then washed three times with 1 mL PBS to clean unlabeled sEVs. The LD column was removed and placed in a 15 mL collection tube. PBS (3 mL) was added to the column, and the magnetic mixture containing labeled sEVs was pushed into the tube by a plunger. The mixture was centrifuged at 100,000 $\times$ g for 70 min, and the precipitates were resuspended in 100  $\mu$ L of PBS. Then, 100  $\mu$ L of elution buffer (0.1 M glycine pH 2.8) was used to dilute the labeled sEV suspension, which was vortexed for 30 s, and combined with 10  $\mu$ L of renaturation buffer (1 M Tris-HCl, pH 7.4). The mixture was centrifuged at 10,000 $\times$ g

for 30 min to separate the sEVs from magnetic beads. The supernatant containing specific sEVs was stored at -80 °C for RNA extraction.

#### Transmission electron microscopy (TEM)

sEVs fixed in 1% paraformaldehyde for 10 min and washed with deionized water. The sEV suspension (10  $\mu$ L) was placed over a Formvar-carbon-coated 300-mesh copper net and incubated for 10 min at room temperature. After washing with deionized water, the sEVs were negatively stained with 2% uranyl oxalate solution for 1 min at room temperature. The grids were dried for 5 min under incandescent light. Images of sEVs were acquired with an FEI Tecnai G2 Spirit Transmission Electron Microscope (TEM) (FEI; Houston, TX, USA).

#### Nanoparticle tracking analysis (NTA)

Based on the characteristics of the Brownian motion and light scattering, the hydrodynamic diameter and concentration of sEVs were measured by NTA (ZetaView PWX 110, Particle Metrix, Germany). sEVs were diluted to 1 mL with PBS and injected into the cuvette. The hydrodynamic diameter and concentration of particles were calculated from the diffusion coefficient by the Stokes-Einstein equation. Five videos of approximately 10 s duration each were recorded for every sample, and analysis of the data regarding particle movement was by the nanoparticle tracking analysis (NTA) software.

#### Western blotting

Protein quantification of sEVs samples was conducted using the BCA Protein Assay Kit (Thermo Fisher Scientific, No. 23,225, USA). The primary antibodies used were CD9 (Abcam, ab92726), CD63 (Abcam, ab216130), CD81 (Abcam, ab109201), TSG101 (Abcam, ab125011), HSP70 (Abcam, ab2787), calnexin (Abcam, ab22595), EpCAM (Abcam, ab32392), FAP (Abcam, ab207178), CD31 (Abcam, ab9498), CD45 (Abcam, ab40763), and  $\beta$ -actin (Proteintech, 66,009--1-Ig). For secondary antibodies, goat anti-rabbit (A0208, Beyotime) and goat anti-mouse (A0216, Beyotime) IgG horseradish peroxidase were used.

#### High-throughput sequencing and differential expression analysis

Total RNA extracted from sEVs of 2 mL plasma was used for miRNA library preparation (Ribobio, China). The clean reads (17–45 nt) were contrasted with human genome databases (Silva, GtRNAdb, Rfam, and Rfam) using the Bowtie software [20]. The clean reads were further compared with mature miRNAs in the miRDeep2 and miRBase databases. Next, the miRNA expression levels were normalized by the RPM. The significant

differential expression analysis of miRNAs was conducted using the edgeR and limma packages.

#### **RNase treatment of sEVs and RNA extraction**

The plasma from the same patient was divided into 3 equal parts. One of which extracted sEV fractions was treated with RNase A (10 µg/mL, Tiangen, No. RT405, China), which is used to eliminate the free RNA carried by non-vesicles, for 15 min at 37 °C. The remaining two plasma samples were not digested with RNase, one of which was directly used to extract plasma RNA, and the other was used to extract RNA from sEVs.

According to the standard protocol, total RNA from plasma or sEVs was extracted and purified by the miRNeasy Serum/Plasma Advanced Kit (Qiagen, No. 217,204, USA). Total RNA from tissue was extracted via a miRNeasy Mini Kit (Qiagen, No. 217004, USA). RNA degradation and contamination were detected by gel electrophoresis. The integrity of RNA was assessed on an Agilent 2200 TapeStation (Agilent Technologies, CA, USA). Additionally, RNA samples were quantified by Qubit<sup>®</sup>2.0 (Life Technologies, USA).

#### **Quantitative real-time PCR (qRT-PCR)**

*C. elegans* cel-miR-39 was used as an external calibration, and U6 was used as an internal reference for tissue and tissue sEV samples. miRNA quantification was performed by a Light Cycler 480 (Roche, Germany) using specific miRNA TaqMan gene expression probes (Synbio Technologies, China) mixed with cDNA templates (Takara, RR037A, Japan). The relative expression levels of candidate miRNAs were normalized to the control group via the Eq.  $2^{-\Delta\Delta Ct}$  [21]. The primer and probe sequences of the miRNAs were listed in Additional file 1: Table S3.

#### **Pathway enrichment analysis**

Target genes of miRNAs were screened via TargetScan and miRWalk. The Tothill dataset (GSE61568) [22] was used to establish the miRNA-gene regulatory network and perform pathway analysis. Tumor cases with low malignant potential, non-serous histology, or low grade from the Tothill dataset were excluded. Samples that received NACT or did not provide residual disease status were excluded. Accordingly, miRNA target genes were matched using only data from primary tumors of patients with HGSOE undergoing surgery in the Tothill dataset. The DAVID website (<https://david.ncifcrf.gov>) was used to conduct functional clustering and enrichment pathway analysis. We classified the GO and KEGG pathways using the two-sided Fisher's exact test and calculated FDR to correct P values. A corrected P value < 0.05 was considered to be significantly enriched in the GO/KEGG

pathway. GSEA was performed by GSEA software (<http://software.broadinstitute.org/gsea/>).

#### **Statistical analysis and prediction model building**

LASSO analysis was performed to select the most relevant predictors via the "glmnet" (strictly set alpha=1) package. Based on the R0 group as a control, we calculated the relative expression abundance of selected miRNAs in the non-R0 and differential diagnostic groups (BPD, ESOC, ACC). Log2 transformation of 4-miRNA qRT-PCR expression values of all samples was completed using the  $\log(x+1, 2)$  formula [11, 23]. Serum CA-125 expression values were converted via log10. We preliminarily fitted the model using logistic regression, as described in refs. [11, 24]. Based on this multivariate logistic regression model, we calculated the risk probability of residual disease for each subject through leave-one-out cross-validation. Moreover, the index score of differential diagnostic patients was also calculated by this risk model. We assessed the optimal cutoff value of the above prediction probability (4-miRNA combined CA-125) by receiver operating characteristic (ROC) curves and calculated sensitivity, specificity, AUC, PPV, and NPV in the discovery set [23]. While using the same cutoff value of risk prediction, the corresponding sensitivity, specificity, AUC, PPV, and NPV were calculated by the ROC curve in the validation set. The NRI and IDI were calculated by R software to quantify the improvement of diagnostic separation [25]. Furthermore, DCA was conducted by the "rmda" package in R. Gpower software was used to calculate the post hoc power of the prediction model. Multivariate and univariate logistic regression were employed to analyze the influence of various clinicopathological variables on residual disease status, including age, stage, lymph node metastasis, TP53 mutation, serum CA-125 levels, and 4-miRNA panel.

For all cohorts, MedCalc statistical software, version 19.1.0 (Medcalc Software, Ostend, Belgium) was used for the calculation and visualization of ROC curve relative indicators [24]. Statistical analysis was carried out using SPSS, GraphPad Prism 8, and R software (version 3.6.3). Comparisons between groups were performed using an unpaired t test or Mann-Whitney U test. The limit of significance was defined as a P value < 0.05. The results were visualized via the R packages VennDiagram, pheatmap, GOplot, and ggplot2.

#### **Data availability statement**

RNA sequence data of all samples were publicly stored in the Gene Expression Omnibus of NCBI, GSE223126 (<https://www.ncbi.nlm.nih.gov/geo/query/acc.cgi?acc=GSE223126>). The accession numbers of previously

published datasets involved in our study were GSE113486 [26], GSE94533 [27], and GSE61568 [22].

## Results

### Assay design and clinical characteristics

A total of 284 pretreatment plasma samples and 76 surgical tissue samples were collected in this study (Fig. 1A). We sought to find a reliable panel for residual disease risk detection in AOC patients. Our design of the three-phase study is shown in Fig. 1B, Additional file 1 Figure S1. Concretely, a total of 284 patients from 4 clinical centers were included in the initial analysis, including 99 AOC patients without any residual disease (R0), 122 AOC patients with any residual disease (non-R0), 20 early-stage OC patients, 21 benign pelvic disease patients, and 22 advanced colorectal cancer patients. Using these samples, we constructed three cohorts: a screening cohort (n=37), a discovery cohort (n=30), and a validation cohort (n=154).

### Plasma sEV-derived miRNA profile in AOC patients

To focus on the sEVs released from AOC patients, we first determined the presence of vesicles within the plasma of AOC patients using electron microscopy. Transmission electron microscopy (TEM) images showed that large and small vesicles isolated from AOC patients' plasma had completely different sizes (Fig. 2A). There were also obvious differences in the diameter ranges of large and small vesicles via nanoparticle tracking analysis (NTA) (Fig. 2B). Furthermore, we found that the large vesicles harbored visible peaks for the 28S ribosomal RNA and a narrower peak for small-RNAs, while small vesicles had a broader small-RNA peak as determined by high-resolution electrophoresis (Agilent 2100 Bioanalyzer) (Fig. 2C). The typical sEV marker proteins CD9, CD63, CD81, TSG101, and HSP70 were also detected in our isolated vesicles, whereas the negative marker protein, calnexin, was absent (Additional file 1: Figure S2). These data proved that the extracted vesicles were extracellular and that miRNAs were mostly derived from small extracellular vesicles (sEVs).

To identify a global expression profile of circulating sEVs-derived miRNAs between non-R0 and R0 patients, we tested 37 AOC patient samples in the screening set (R0, n=17; non-R0, n=20) using small RNA sequencing. In all samples, we detected 1832 known miRNAs, and 151 differentially expressed miRNAs (DEMs) between the two groups ( $|\log_2(\text{FC})| > 1$  and  $P < 0.05$ ) (Fig. 3A). To avoid the bias in the differential analysis caused by miRNAs with low expression, 51 DEMs (42 upregulated; 9 downregulated) with an average RPM > 50 was chosen from 151 DEMs as candidate miRNAs (Fig. 3B). The log (FC) value and the P value of these 51 selected DEMs

are included in Additional file 1: Table S1. Unsupervised cluster heatmap and principal component analysis (PCA) further identified that these 51 DEMs could distinguish non-R0 subjects from R0 subjects (Fig. 3B, C). Moreover, the driver genes of HGSOE (TP53, PTEN, BRAC, RB1, etc.) have been recognized and published in Nature [28, 29]. 15 miRNAs targeting these driver genes were further filtered from 51 DEMs.

### Construction of a prediction model using plasma sEV-derived miRNAs and CA-125 in the discovery set

In the independent discovery set consisting of 30 AOC patients (R0, n=15; non-R0, n=15), we examined the diagnostic robustness of the above 15 selected miRNAs by TaqMan qRT-PCR for further screening of miRNAs with expressed commonality in order to exclude the influence of individual differences. The qRT-PCR data illustrated that 15 miRNAs had a potential co-regulation ( $r > 0.6$ ) (Fig. 4A). The fold change, P value, and area under the receiver-operator characteristic (ROC) curve (AUC) of 15 miRNAs are shown in Additional file 1: Table S2. Then, we screened 8 miRNAs with significant differences from 15 miRNAs in the discovery set (Additional file 1: Table S2). Since the diagnostic performance of a single miRNA was relatively low (AUC: 0.58~0.78), we planned to use multiple miRNAs combined with clinical serum biomarkers to develop the prediction model.

To obtain better performance parameters and avoid overfitting the model, the best risk /predictive panel containing 4 miRNAs from the above 8 miRNAs was selected by least absolute shrinkage and selection operator (LASSO) regression (penalized coefficients,  $\lambda = 0.07$ ) (Fig. 4B, C). The LASSO coefficient of 4-miRNA is displayed in Fig. 4D. Consistent with clinical application, CA-125 is an initial and important clinical biomarker of AOC [30], as CA-125 (AUC: 0.662) showed relatively higher diagnostic performance than CA-153 (AUC: 0.567) and CA-199 (AUC: 0.533) in distinguishing non-R0 from R0 patients (Fig. 4E). Interestingly, a new combination signature of 4-miRNA and CA-125 (AUC: 0.973, 95% CI 0.838~1.000) demonstrated a higher detection accuracy than the 4-miRNA panel (AUC: 0.969) or CA-125 alone (AUC: 0.662) (Fig. 4E, F), just as serum CA19-9 could also improve the diagnostic performance of the miRNA biomarker panel for detecting gastric cancer [31] or pancreatic adenocarcinoma [32]. The indicators related to the ROC of the above predictors are shown in Table 2. The risk score model of 4-miRNA and CA-125 was established by logistic regression analysis as follows: Index mC = miR-320a-3p\*(0.179) + miR-378a-3p\*(0.067) + miR-1307-3p\*(0.052) + let-7d-3p\*(-0.198) + CA-125\*(0.122) + 0.701 (cutoff = 1.483). If the index mC of AOC patients is higher than the cutoff

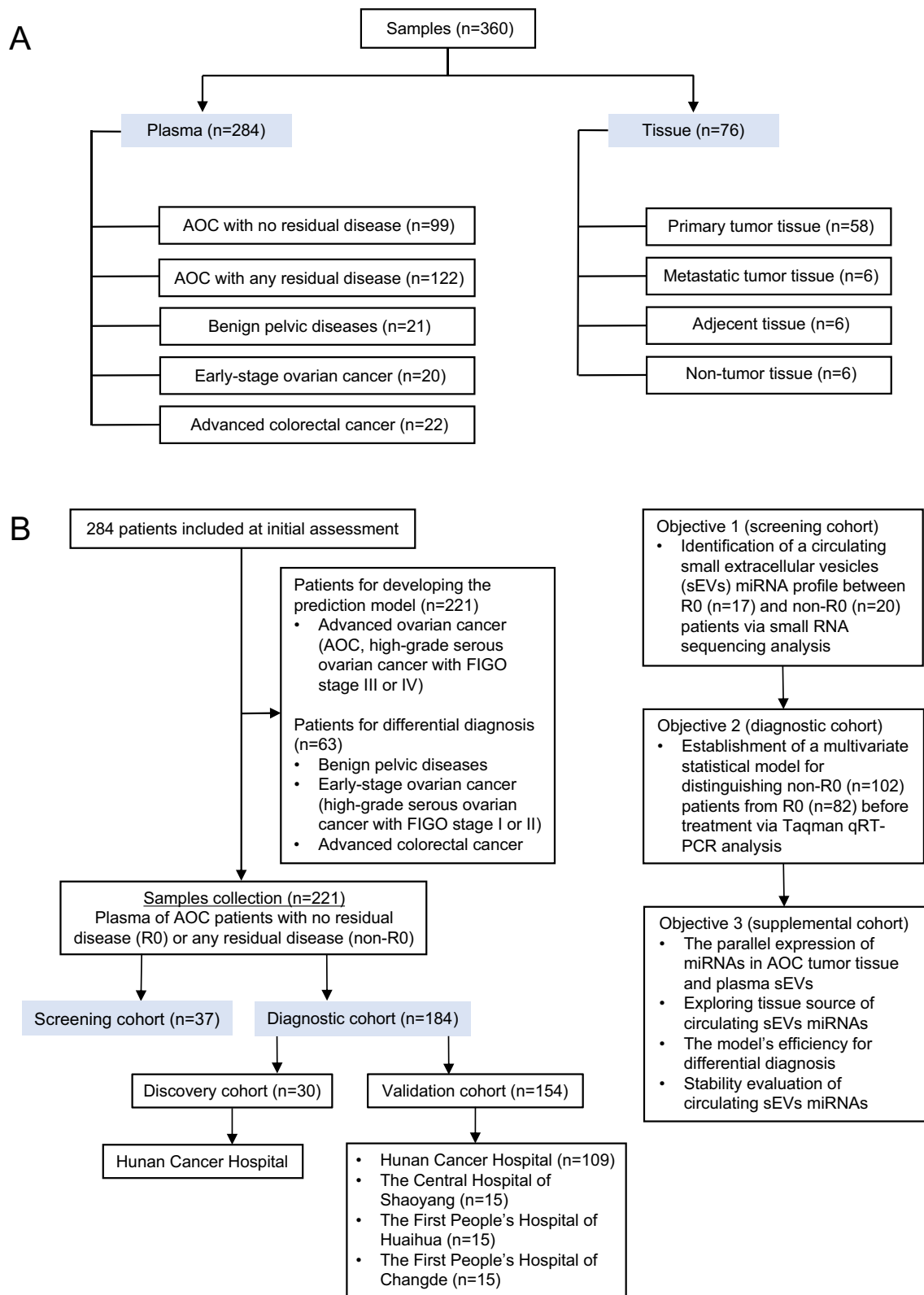


**Fig. 1** Assay design and clinical characteristics **A:** A total of 360 plasma and tissue samples were tested in our study. **B:** Flowchart of study design was prepared to establish a diagnostic model for predicting residual disease risk in AOC patients. AOC advanced ovarian cancer

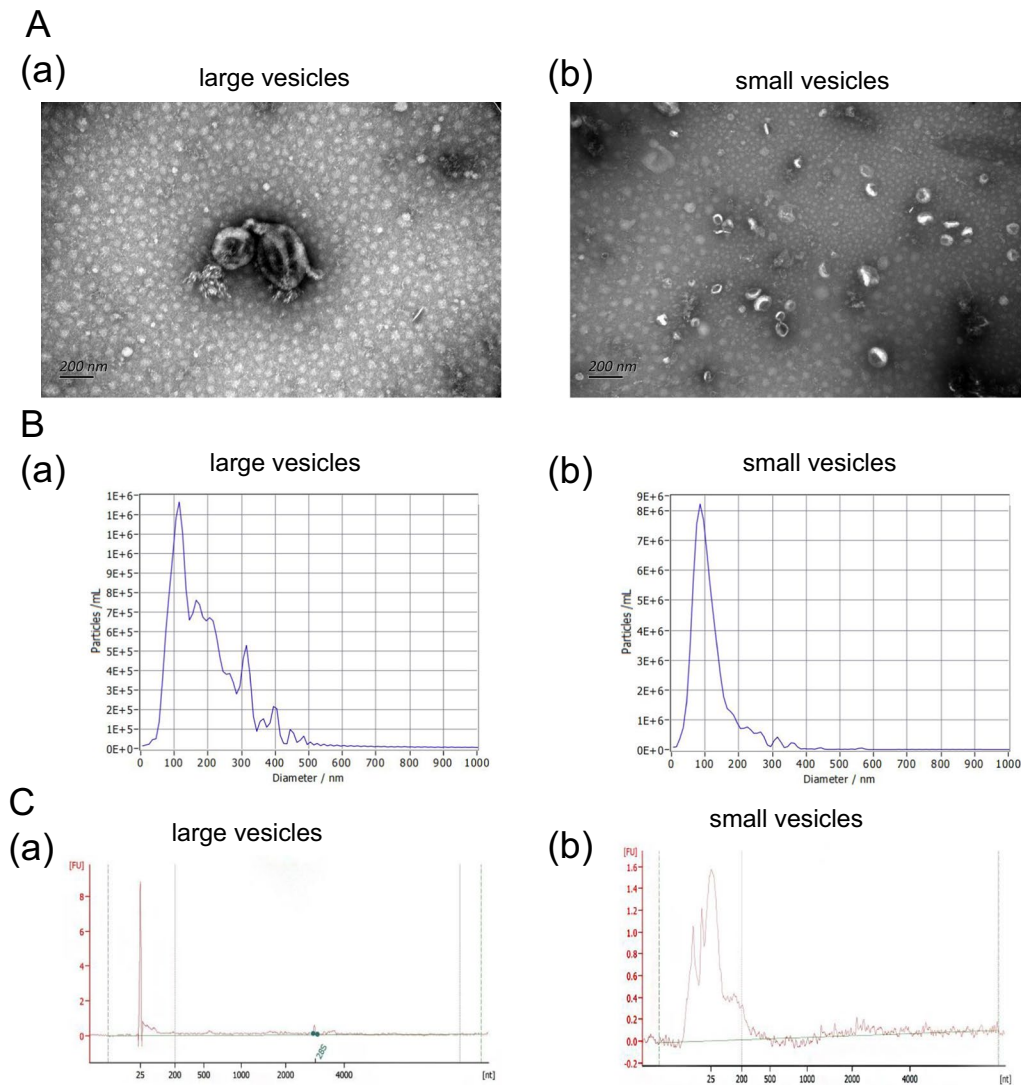


**Fig. 2** Characterization of large and small EVs isolated from AOC tissues. **A:** 10 micro-liters of large **a** and small vesicles **b** from AOC tissues were loaded onto grids, negative stained, and evaluated with transmission electron microscopy (TEM). Scale bars, 200 nm. **B:** Size distribution of large **a** and small vesicles **b** were obtained using nanoparticle tracking analysis (NTA; ZetaView®). Size distribution is presented as graphs with the concentration of the structures on the y-axis and the diameter of the structures in nanometres on the x-axis. **C:** RNA of large **a** and small vesicles **b** were isolated directly from the EV pellets and was analysed with a Bioanalyzer® (Agilent 2100). AOC advanced ovarian cancer

value, they would be defined as high-risk patients with residual disease.

**Combining 4-miRNA with CA-125 for R0 and non-R0 patient categorization in the validation set**

Next, we evaluated the accuracy of this statistical model in the independent validation set (R0, n=67; non-R0, n=87). Compared to 4-miRNA, CA-125, CA-153, or CA-199 alone, the combined model had the highest diagnostic utility (AUC: 0.903, 95% CI 0.846 ~ 0.945, Fig. 5A, B).

Notably, cases in our diagnostic cohort (Fig. 1B) initially erroneously discriminated by CA-125 or 4-miRNA panel were significantly reduced after reclassification by our prediction model (Fig. 5C, D). The positive predictive value (PPV=0.926) and negative predictive value (NPV=0.871) of this model were significantly increased compared to CA-125 (PPV=0.706; NPV=0.712) (Table 1). Decision curve analysis (DCA) indicated that the decision utility of 4-miRNA combined CA-125 for defining high-risk groups was superior to CA-125 or 4-miRNA alone (Fig. 5E). The quantitative evaluation of net reclassification improvement (NRI) and integrated

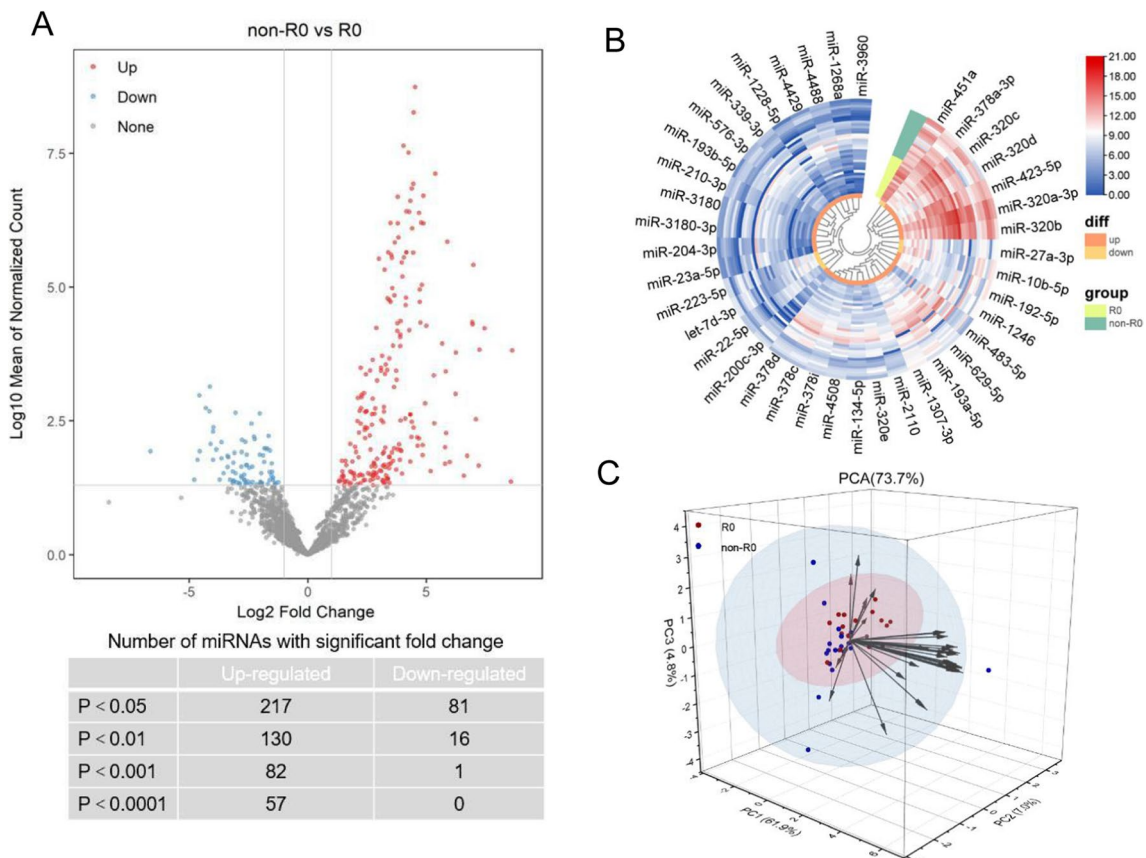


**Fig. 3** Plasma sEVs derived miRNA profile in AOC patients **A**: Volcano plot showed all DEMs between non-R0 (n=20) and R0 (n=17) groups in small RNA sequencing. The red and blue represented the up-regulated and down-regulated DEMs, respectively. ( $|\log_2(FC)| > 1, P < 0.05$ ); The table summarized the numbers of DEMs defined by different P values. **B**: A heatmap of 51 DEMs expressions in miRNA-seq data. **C**: Principal component analysis of 51 DEMs expressions between non-R0 and R0 groups. *miRNA* microRNA, *sEVs* small extracellular vesicles, *AOC* advanced ovarian cancer, *DEMs* differentially expressed miRNAs, *R0* advanced ovarian cancer with no residual disease, *non-R0* advanced ovarian cancer with any residual disease

discrimination improvement (IDI) further showed that the additional predictive power of our combined model for the residual disease was significantly improved compared with CA-125 or 4-miRNA alone (model vs CA-125, NRI=0.471,  $P < 0.001$ ; IDI=0.538,  $P < 0.001$ ; model vs 4-miRNA panel, NRI=0.122,  $P = 0.001$ ; IDI=0.185,  $P = 0.003$ ) (Table 2). Pairwise comparison of ROC curves

showed that the increased AUC value of the combined model had statistical significance compared with CA-125 (AUC: 0.914, 0.679;  $P < 0.0001$ ) or 4-miRNA (AUC: 0.914, 0.853;  $P = 0.0007$ ) (Table 2).

To further assess the model developed herein, we investigated the influence of patient backgrounds. Through postsurgical pathological reports, we found that

(See figure on next page.)

**Fig. 4** Construction of a prediction model using plasma sEVs derived miRNAs and CA-125 in the discovery set **A**: Pearson correlation analysis of 15 selected miRNAs levels detected by Taqman qRT-PCR in the discovery set (R0, n=15; non-R0, n=15). Pearson correlation coefficient and P value were displayed in the bottom-left and the upper-right, respectively. **B**: The  $\log(\lambda)$  was plotted versus AUC. Numbers along the upper x-axis indicated the number of predicted factors. The black vertical lines defined the optimal values of  $\lambda$  ( $\lambda = 0.07$ ), where the model provided the best fitting to the data; **C**: The LASSO coefficient profile plot of the selected 4 texture features (miR-320a-3p, miR-378a-3p, miR-1307-3p, let-7d-3p). **D**: The LASSO coefficient values of 4 miRNAs. **E-F**: The ROC curves of (**E**) 4-miRNA panel, CA-125, CA-153, CA-199, and (**F**) 4-miRNA combined with CA-125 for detecting residual disease in the discovery set. Maximum classification accuracy was labeled by the red circle. *miRNA* microRNA, *sEVs* small extracellular vesicles, *R0* advanced ovarian cancer with no residual disease, *non-R0* advanced ovarian cancer with any residual disease, *LASSO* least absolute shrinkage and selection operator, *AUC* area under the receiver operating characteristic curve, *ROC* receiver operating characteristic curve; \* $P < 0.05$ ; \*\* $< 0.01$ ; \*\*\* $< 0.001$ ; \*\*\*\* $< 0.0001$



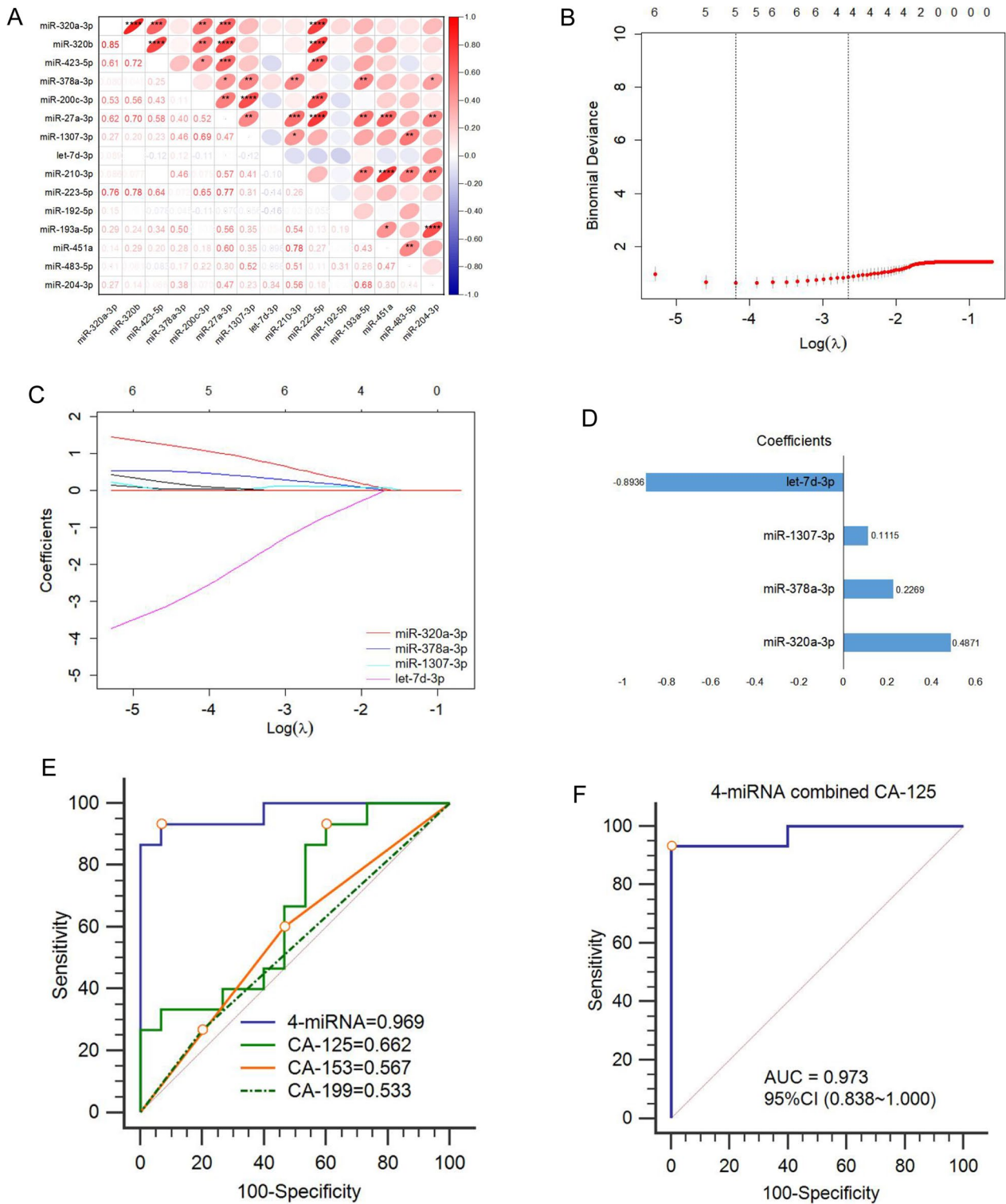


**Fig. 4** (See legend on previous page.)

non-R0 and R0 AOC cases were differed for stage, lymph node metastasis, and serum CA-125 levels, whereas age and P53 mutation did not differ significantly (Table 3,

Additional file 1: Table S4–S6). Additionally, multivariate logistic regression analysis revealed that our newly developed 4-miRNA panel emerged as an independent risk

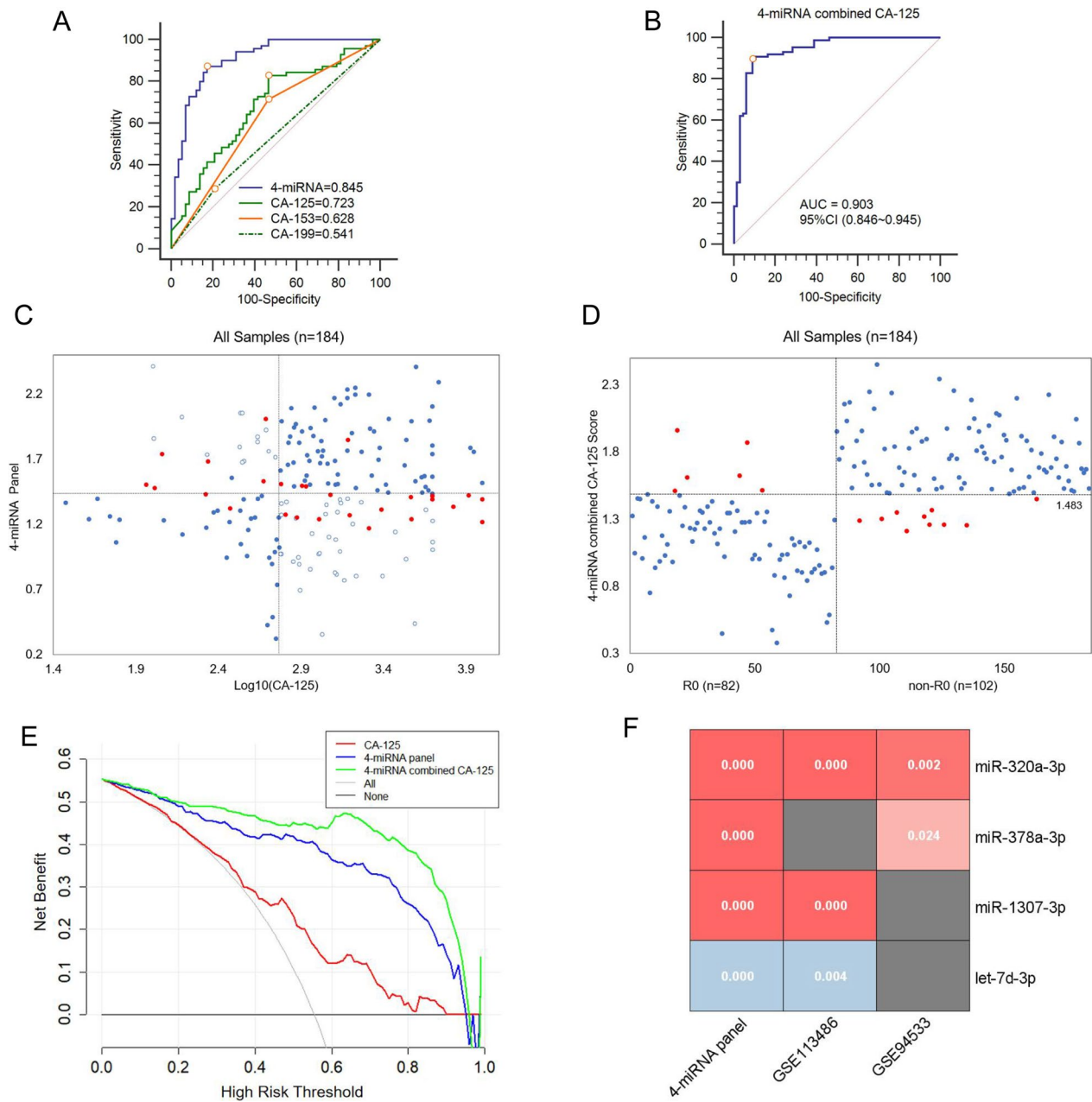


**Fig. 5** Combining 4-miRNA with CA-125 for R0 and non-R0 patients categorization in the validation set **A–B**: The ROC curves of **A** 4-miRNA panel, CA-125, CA-153, CA-199, and **B** 4-miRNA combined with CA-125 for detecting residual disease in the validation set (R0, n=67; non-R0, n=87). Maximum classification accuracy was labeled by the red circle. **C**: The 2-dimensional classified plot of the 4-miRNA panel score (y-axis) and serum log10(CA-125) level (x-axis) for all subjects in the discovery and validation sets (n=184). The horizontal and vertical dashed lines represented the classification threshold of the 4-miRNA panel (1.422) and CA-125 (600 U/ml), respectively. The misclassified cases via 4-miRNA panel or CA-125 were marked with a red point (n=27) or a blue circle (n=59), respectively. **D**: The 2-dimensional classified plot of the prediction model combining 4-miRNA with CA-125 for all subjects in the discovery and validation sets (n=184). The horizontal dashed line was the classification threshold (1.483) of the combined model. The false-positive and false-negative cases were in red (n=16). **E**: The decision curve analysis (DCA) plot of three models (CA-125, 4-miRNA, 4-miRNA combined with CA-125) (n=184). **F**: The P value list of differentially expressed 4-miRNA in our panel and public datasets (GSE113486, GSE94533). Red marked up-regulated miRNAs and blue marked down-regulated miRNAs. miRNA, microRNA; ROC receiver operating characteristic curve, R0, advanced ovarian cancer with no residual disease, non-R0 advanced ovarian cancer with any residual disease; \*P < 0.05, \*\* < 0.01, \*\*\* < 0.001, \*\*\*\* < 0.0001

**Table 1** Performance of CA-125, 4 miRNAs, 4-miRNA panel, and 4-miRNA combined with CA-125 for predicting residual disease

Biomarker	Performance	Discovery set (n = 30)	Validation set (n = 154)
miR-320a-3p	Sensitivity	100	81.6
	Specificity	53.3	62.7
	PPV	65.2	80.0
	NPV	100	72.4
	AUC	75.6	77.2
miR-378a-3p	Sensitivity	66.7	87.4
	Specificity	80.0	50.7
	PPV	76.9	69.7
	NPV	70.6	75.6
	AUC	74.7	75.1
miR-1307-3p	Sensitivity	66.7	57.5
	Specificity	86.7	77.6
	PPV	76.9	76.1
	NPV	70.6	58.6
	AUC	77.6	68.2
let-7d-3p	Sensitivity	73.3	78.2
	Specificity	66.7	65.7
	PPV	68.8	74.2
	NPV	71.4	67.7
	AUC	69.3	78.4
4-miRNA panel	Sensitivity	93.3	83.9
	Specificity	93.3	85.1
	PPV	87.5	88.0
	NPV	92.9	80.3
	AUC	96.9	84.5
CA-125	Sensitivity	93.3	82.8
	Specificity	40.0	56.7
	PPV	50.0	70.6
	NPV	83.3	71.2
	AUC	66.2	72.3
CA-125 + 4-miRNA panel	Sensitivity	93.3	89.7
	Specificity	100.0	91.0
	PPV	100.0	92.6
	NPV	93.8	87.1
	AUC	97.3	90.3

The sensitivity, specificity, PPV positive predictive value, NPV negative predictive value and area under the curve (AUC) are shown as % (simple counts)

feature for residual disease in both clinical cohorts (discovery set: OR=2.415; 95% CI 1.779~3.279;  $P < 0.0001$ , validation set: OR=1.866; 95% CI 1.649~2.110;  $P < 0.0001$ , Table 3). The post hoc power of our model was above 0.9. Circulating 4-miRNA expression was also significantly different between the OC and normal groups according to analysis of public datasets (GSE113486 and GSE94533) (Fig. 5F). These results indicated that the combining model of 4-miRNA and CA-125 represented a promising classifier for residual disease detection.

#### Tumor cell-derived sEV miRNAs contribute to the plasma sEV miRNAs signature in AOC patients

Interestingly, the expression trend of 4-miRNA in tumor tissues of AOC patients was consistent with that in circulating sEVs (Fig. 6A). In addition, for testing the differential diagnostic ability of this model, we calculated the model index score of patients with benign pelvic diseases (BPD), early-stage ovarian cancer with FIGO I or II (ESOC), and advanced colorectal cancer (ACC). Surprisingly, the model index scores of the above patients were significantly lower than AOC patients (Fig. 6B). Thus, we further investigated 4-miRNA expressions in different tissue-derived sEVs. The isolated tissue vesicles were sEVs based on characterization analysis (Additional file 1: Figures S3 and S4). The expression levels of 3 up-regulated miRNAs (miR-320a-3p, miR-378a-3p, miR-1307-3p) in primary tumor tissue (PTT) and metastatic tumor tissue (MTT)-derived tissue-sEVs were significantly higher than those in adjacent tissue (AT) and non-tumor tissue (NTT) groups, while let-7d-3p expression presented a reverse trend (Fig. 6C). There was no significant difference between PTT and MTT groups. These results demonstrated that sEVs 4-miRNA expressions were mainly affected by tumor tissue or tumor microenvironment.

We then detected the enrichment of known celltype-specific markers in the tumor tissue-sEV pool by western blot. EpCAM (epithelial cell adhesion molecule) [33], a transmembrane protein often overexpressed in epithelial carcinomas, was chosen as the epithelial ovarian cancer cells (EOCC) marker; FAP (fibroblast activation protein) [34] as the cancer-associated fibroblasts (CAFs) marker; CD31 [35] as the endothelial cells (ECs) marker and CD45 [36] as the tumor-infiltrating immune cells (TICs)

**Table 2** Reclassification of the prediction model (4-miRNA combined CA-125) compared to CA-125 or 4-miRNA panel alone in subjects (n = 184)

Model	CA-125	CA-125 + 4-miRNA panel	P value	4-miRNA panel	4-miRNA panel + CA-125	P value
AUC	0.679	0.914	<b>&lt; 0.0001</b>	0.853	0.914	<b>0.0007</b>
NRI	0.471		<b>&lt; 0.001</b>	0.122		<b>0.001</b>
IDI	0.538		<b>&lt; 0.001</b>	0.185		<b>0.003</b>

Significant P values in bold; IDI Integrated Discrimination Improvement, NRI net reclassification improvement

**Table 3** Univariate and multivariate logistic regression analysis for residual disease in the discovery and validation cohorts

	Discovery set (n = 30)			Validation set (n = 154)		
	OR	95% CI	P value	OR	95% CI	P value
Univariate logistic regression analysis						
Age (years) (≥ 60 vs. < 60)	0.375	0.073~1.920	0.229	0.795	0.390~1.622	0.529
Stage (IV vs. III)	5.091	0.496~52.287	0.130	10.601	3.537~31.775	< 0.0001
Lymph node metastasis (positive vs. negative)	1.375	0.286~6.603	0.690	2.561	1.275~5.144	0.0075
P53 mutation (Positive vs. Negative)	0.762	0.179~3.241	0.712	1.167	0.519~2.623	0.710
Serum CA-125 (≥ 600 vs. < 600 U/ml)	5.688	0.939~34.458	0.042	4.767	2.261~10.054	< 0.0001
4-miRNA panel (High vs. Low risk)	91	7.348~1126.947	< 0.0001	29.721	12.299~71.826	< 0.0001
Multivariate logistic regression analysis						
Age (years) (≥ 60 vs. < 60)	1.156	0.862~1.551	0.342	0.963	0.844~1.100	0.581
Stage (IV vs. III)	0.863	0.597~1.247	0.441	1.169	1.005~1.359	0.045
Lymph node metastasis (Positive vs. Negative)	1.048	0.787~1.395	0.753	1.142	1.005~1.297	0.044
P53 mutation (Positive vs. Negative)	0.952	0.740~1.226	0.709	1.030	0.899~1.180	0.672
Serum CA-125 (≥ 600 vs. < 600 U/ml)	1.047	0.785~1.395	0.759	1.249	1.096~1.424	0.001
4-miRNA panel (High vs. low risk)	2.415	1.779~3.279	< 0.0001	1.866	1.649~2.110	< 0.0001

Significant P values in bold, OR odds ratio, CI confidence interval

marker. We observed that EpCAM, FAP, and CD31 were expressed abundantly in tissue-derived sEV fractions, whereas CD45 was almost undetectable (Fig. 6D). The results showed that the tumor tissue-sEVs pool was a relatively mixed environment, where EOCCs, CAFs, and ECs-derived sEVs were the main contributors, whereas TICs-derived sEVs were not enriched. We further sorted tissue-derived EVs from EOCCs, CAFs, and ECs by an immunoaffinity magnetic bead sorting system (MACS). Surprisingly, the expression levels of the 3 upregulated miRNAs in the EOCCs group were higher than those in the CAFs, and ECs groups, whereas let-7d-3p expression in the EOCCs group was the lowest (Fig. 6E).

Meanwhile, we were more interested in understanding the source of sEV 4-miRNA directly from circulation and excluding the effects of circulating confounders. EpCAM has long been utilized to detect circulating epithelial tumor cells [37] and their derived sEVs [13]. Previous

studies showed that most circulating sEVs concentrated by ultracentrifugation in platelet-depleted plasma originated from erythrocytes and leukocytes rather than platelets or megakaryocytes as commonly thought [38]. CD235a and CD45 were assessed as erythrocyte and leukocyte markers, respectively. We captured plasma sEVs by MACS with these specific proteins. 3 up-regulated miRNAs were packaged at high concentrations in EOCCs-derived plasma EpCAM+ -sEVs, while these were not detected in erythrocytes and leukocyte-derived sEV samples (Fig. 6F). Let-7d-3p expression was the lowest in the EOCCs group (Fig. 6F). Collectively, the differential expression of plasma sEV-derived 4-miRNA between the R0 and non-R0 groups was mainly dominated by tumor cells.

The Agilent 2100 Bioanalyzer results showed that the RNA content derived from plasma sEVs was decreased by about 55% compared with RNA extracted directly

(See figure on next page.)

**Fig. 6** Tumor cells-derived sEVs miRNAs contribute to plasma sEVs miRNAs signature in AOC patients **A:** The 4-miRNA expressions in tumor tissue between two groups were verified by Taqman qRT-PCR (R0, n = 20; non-R0, n = 30). **B:** The 4-miRNA expressions in sEVs derived from primary tumor tissue (PTT, n = 6), metastatic tumor tissue (MTT, n = 6), adjacent tissue (AT, n = 6), or non-tumor tissue (NTT, n = 6) via Taqman qRT-PCR. **C:** Representative western blots of cell-type-specific protein in primary tumor tissue sEVs (n = 6); **D:** Taqman qRT-PCR analysis of 4-miRNA in different cell-source sEVs separated from primary tumor tissue (n = 3); **E:** Taqman qRT-PCR analysis of 4-miRNA in plasma different cell-source sEVs captured by magnetic beads sorting system (n = 6); EpCAM was chosen as epithelial ovarian cancer cells marker; FAP as cancer-associated fibroblasts marker; CD31 as endothelial cells marker; CD45 as tumor-infiltrating immune cells and leukocytes marker; CD235a as erythrocytes marker. **F:** The comparison of model index score between R0 (n = 82) or non-R0 (n = 102) patients and benign pelvic diseases (BPD, n = 21), early-stage ovarian cancer with FIGO I or II (ESOC, n = 20), and advanced colorectal cancer patients (ACC, n = 22). **G:** The relative expression levels of miR-320a-3p, miR-378a-3p, miR-1307-3p, let-7d-3p were detected from total plasma, plasma sEVs, and plasma sEVs pretreating with RNase A. miRNA, microRNA; R0, advanced ovarian cancer with no residual disease; non-R0, advanced ovarian cancer with any residual disease; sEVs, small extracellular vesicles; AOC, advanced ovarian cancer; \*P < 0.05; \*\* < 0.01; \*\*\* < 0.001; \*\*\*\* < 0.0001 (unpaired t-test)

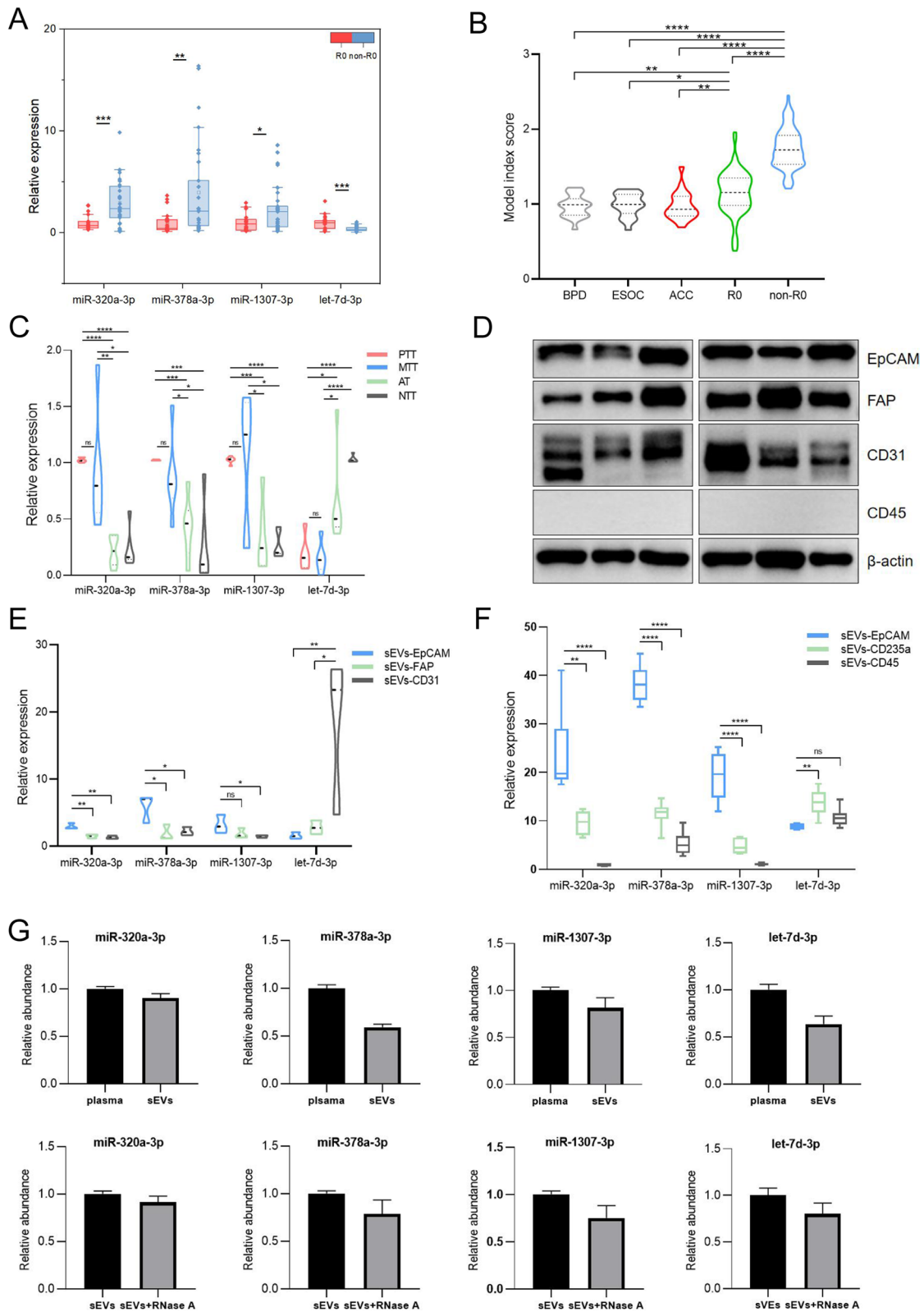


**Fig. 6** (See legend on previous page.)

from total plasma, whereas RNA derived from plasma sEVs treated with RNase A was slightly decreased by about 13% (Additional file 1: Figure S5). Moreover, the RNase degradation assay showed that circulating miR-320a-3p and miR-1307-3p mainly existed in a sEVs manner, while a small part of miR-378a-3p and let-7d-3p was a free-form, and 4-miRNA in sEVs was largely not degraded after treatment with RNase A (Fig. 6G). These results revealed that circulating sEV 4-miRNA was sufficient stable and excluded possible contamination with non-sEV miRNAs during the extraction procedure.

#### Target gene prediction and pathway enrichment analysis of the multi-miRNA panel

Furthermore, we found 2701 target genes of 4 miRNAs in common between the TargetScan, miWalk, and residual disease-associated tissue datasets (Tothill dataset, GSE61568) (Fig. 7A). 4-miRNA target genes (*TP53TG3*, *RBI*, *CCNE1*, *CSMD1*) closely related to HGSOc were significantly differentially expressed between the R0 and non-R0 groups in the Tothill dataset (Fig. 7B). Gene Ontology (GO) analysis showed that these mRNAs were mainly concentrated in the pathways of cell migration and DNA damage repair (Fig. 7C). In addition, we found that the *TP53*, *mTOR*, *FoxO*, and *ErbB*-related signaling pathways were strongly enriched in the Kyoto Encyclopedia of Genes and Genomes (KEGG) pathway categories (Fig. 7D). Gene set enrichment analysis (GSEA) also revealed that these mRNAs were significantly enriched in pathways of cell colonization and adhesion, tumor metastasis, and positive regulation of the protein metabolic process (Fig. 7E). Different but related tumor pathways of miRNA targeting suggested that 4-miRNA expression was closely associated with HGSOc progression from local to metastasis.

#### Discussion

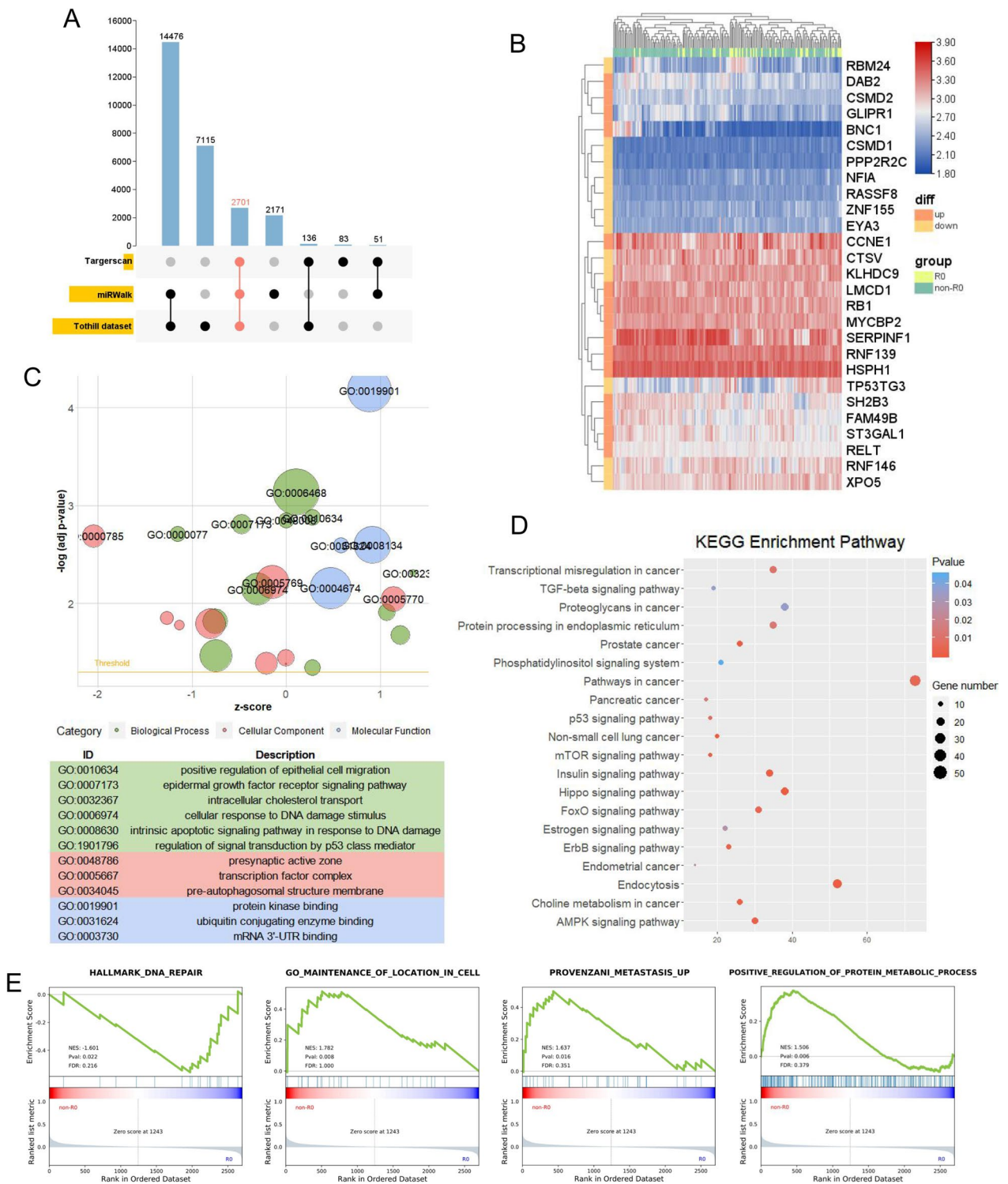
No residual disease after debulking surgery is the most critical independent prognostic factor for AOC. There is an unmet clinical need for selecting primary or interval debulking surgery using existing prediction models. In this study, we discover a distinct sEVs miRNAs

profile between R0 and non-R0 AOC patient. And our aim is to find circulating sEVs miRNAs signature with the most stable expressed commonality among different AOC patients to exclude the influence of individual differences. Therefore, we have enrolled 360 patients from four clinical centers in this study. Based on it, we develop and validate a reliable and stable model of circulating sEVs miRNA panel combined with CA-125 for predicting residual disease risk in AOC patients for the first time. And this combined model can also discriminate diseases easily confounded with AOC (e. g., advanced colorectal cancer). On the other hand, Taqman qRT-PCR detection of the prediction panel is a non-invasive, safe, and easy to perform method, which is helpful for clinical application. Our prediction model can be part of a clinical standard monitoring strategy for screening high-risk AOC patients who are allowed for neoadjuvant chemotherapy instead of PDS.

NACT-IDS is the preferred alternative strategy for 30% of AOC patients with a higher disease burden who have entirely no chance for R0 resection [39]. The platinum-based chemotherapy response rate for HGSOc is as high as 80% [40]. Taylor et al. discovered that circulating tumor exosomal miRNA signatures paralleled and exhibited a strong correlation with tumor tissue-derived miRNA profiles (ranging from 0.71 to 0.90) [13]. Taka-hiro et al. performed the first large-scale comprehensive analysis of circulating miRNAs for the early detection of OC [14]. Their data showed that miRNA levels in early-stage OC were not significantly different from those of borderline and benign tumors, whereas miRNA levels changed dramatically in AOC. Their work revealed that circulating miRNAs could more clearly reflect AOC progression. In terms of exploring residual disease-related biomarkers, Anil K. Sood [41] found that FABP4 and ADH1B were highly expressed in the tumor tissue of non-R0 patients. Although this attempt used objective biomarkers, its limitations included not only the difficulty of obtaining tumor tissue before the operation but also the difference in gene expression rate between metastatic and primary tumor sites. There is currently no consensus on the choice of a specific circulating sEVs-derived

(See figure on next page.)

**Fig. 7** Target genes prediction and pathway enrichment analysis of the multi-miRNA panel **A:** Upset plot of 4-miRNA's target genes via Targetscan, miRWalk, and Tothill dataset. **B:** Expression heatmap of representative 4-miRNA related target genes between R0 (n = 38) and non-R0 (n = 127) groups in the Tothill dataset. Orange represented up-regulated target genes, and yellow represented down-regulated target genes. **C:** GO enrichment analysis of target genes was performed and visualized by GOplot. Log(FC) of selected genes was taken from Tothill dataset. Z-score indicated if the biological process (biological process/cellular components/molecular function) was more likely to be increased (Z-score > 0) or decreased (Z-score < 0). The area of the circles was proportional to the number of genes in the pathway. A threshold was set as log(adj P value) > 2. **D:** A bubble plot of enriched KEGG pathway. **E:** GSEA was performed by the expression of 4-miRNA target genes between R0 and non-R0 groups in Tothill dataset. *miRNA* microRNA, *R0* advanced ovarian cancer with no residual disease; *non-R0* advanced ovarian cancer with any residual disease; *KEGG* Kyoto Encyclopedia of genes and Genomes



miRNA signature to non-invasively predict residual disease in AOC.

Therefore, we performed a systemic and comprehensive analysis of the circulating sEVs miRNAs landscape in R0 and non-R0 subjects. Circulating miRNAs previously identified as diagnostic biomarkers for OC (miR-92, miR-21, miR-221, miR-200c, miR-182) were also highly expressed in our plasma sEVs samples, underlining the validity of our analysis [42]. To maximize the success rate of verification, we narrowed the scope of candidate miRNAs by the following characteristics: (1) high expression abundance; (2) conserved; and (3) targeting HGSOC closely related drive genes. Moreover, patients recruited from four clinical centers enhanced the model's generalization.

FIGO stage and tumor burden were positively correlated with the residual disease risk of AOC patients [43]. In addition, oncogenic perturbations of tumor cells are involved in the alteration of specific miRNA species' content in sEVs, which possibly drives cancer progression and generate novel classes of clinical biomarkers [44]. Our data showed that EOCCs-derived sEVs captured on EpCAM antibody-coated magnetic beads were the major vehicles affecting circulating 4-miRNA expressions. The model index score was positively correlated with the tumor burden of AOC patients. Although we used a novel and improved experimental method, some sEVs were still lost in the sorting process due to existing technical difficulties. Furthermore, according to the expression of miR-1307-3p and let-7d-3p in Fig. 6E, CAFs might also have some influence on panel-miRNA expression. We could not completely preclude that other cells in the tumor microenvironment or other tissues might express circulating sEVs' 4-miRNA. During the processing of plasma samples, anticoagulants, storage temperature, and centrifugation time were strictly controlled to avoid the effects of microvesicles derived from platelet, and hemolyzed samples were removed.

A series of studies reported that circulating miR-320a could also be a potential diagnostic factor in OC [45], prostate cancer [46], and hepatocellular carcinoma [47]. Circulating miR-1307-3p is considered as a diagnostic biomarker of OC [48], breast cancer [49], and gastric cancer [50]. Circulating let-7d often emerged as a diagnostic molecular that is down-regulated in pancreatic cancer [51], hepatocellular carcinoma [52], and cervical cancer [53]. Meanwhile, there have been relatively fewer studies on miR-378a-3p as a cancer biomarker. To pin down the mechanisms and pathogenic relevance of 4-miRNA, further studies will be needed in the future.

CA-125 is dramatically elevated in BPDs such as tuberculous peritonitis and theca follicular fibroma [54]. In addition, ACC with extensive pelvis metastasis is also prone to confusion with AOC; colonoscopy is normally needed to differentiate the two. However, our model could distinguish AOC from these diseases non-invasively (Fig. 6B). Furthermore, a key prerequisite for the molecular signature with a potential clinical application is a fast, robust, and easy-to-perform laboratory assay. Our TaqMan qRT-PCR validation of the circulating sEVs miRNA panel is a vital step in this direction [11, 55]. This testing panel, as an affordable approach, is expected to provide benefits for AOC patients in developing countries.

### Limitations

We will further perform additional survival analysis when the needed terminal events have been reached. Additionally, we collected plasma samples from patients who received NACT after every round of chemotherapy to detect changes in the model index score to further explore the best time for IDS. Meanwhile, we may employ droplet digital PCR in the subsequent clinical transformation.

### Conclusions

Overall, for the first time, we established a reliable and objective model composed of circulating tumor-derived sEVs 4-miRNA and CA-125 for predicting residual disease risk in AOC patients, which could accurately assess the triage of PDS versus NACT-IDS. This model, as a tool for non-invasive liquid biopsy, has great potential to be part of clinical monitoring strategies for screening high-risk patients with residual disease.

### Abbreviations

R0 resection	No: residual disease
AOC	Advanced ovarian cancer
sEVs	Small extracellular vesicles
miRNA	MicroRNAs
LASSO	Least absolute shrinkage and selection operator
NRI	Net reclassification improvement
IDI	Integrated discrimination improvement
PDS	Primary debulking surgery
TEM	Transmission electron microscopy
DEMs	Differentially expressed miRNAs
R0	Advanced ovarian cancer with no residual disease
non-R0	Advanced ovarian cancer with any residual disease
AUC	Area under the receiver operating characteristic curve
ROC	Receiver operating characteristic curve
KEGG	Kyoto Encyclopedia of genes and Genomes



## Supplementary Information

The online version contains supplementary material available at <https://doi.org/10.1186/s12967-023-04774-4>.

**Additional file 1: Table S1.** 51 selected miRNAs ranked by logFC  $\times$  P value (miRNA-seq data). **Table S2.** Fold changes, corresponding P, and AUC values of 15 candidate miRNAs in the discovery cohort. **Table S3.** PCR primer and probe sequences. **Table S4.** Baseline characteristics of the patients in screening cohort. **Table S5.** Baseline characteristics of the patients in discovery cohort. **Table S6.** Baseline characteristics of the patients in validation cohort. **Figure S1.** The flowdiagram of the analysis through the three cohort. **Figure S2.** Identification of sEVs extracted from AOC patients' plasma (western blotting). **Figure S3.** Identification of sEVs extracted from AOC patients' tissue (TEM/NTA). **Figure S4.** Identification of sEVs extracted from AOC patients' tissue (western blotting). **Figure S5.** Plasma content characteristic verification of 4-miRNA.

## Acknowledgements

We thank all study participants and coordinators from the Hunan Cancer Hospital / The Affiliated Cancer Hospital of Xiangya School of Medicine, Central South University, The Central Hospital of Shaoyang, The First People's Hospital of Huaihua / The Affiliated Huaihua Hospital of University of South China, The First People's Hospital of Changde, Northwestern University Feinberg School of Medicine and MD Anderson Cancer Center in the USA, and University College London Hospital in the UK; and thank the nurses as well as colleagues from Gynaecological oncology, and our collaborator team members. We are grateful for the experimental support from the Central Laboratory of Hunan Cancer Hospital and the Cancer Invasion and Metastasis Laboratory of the Cancer Research Institute of Xiangya School of Medicine, Central South University; We particularly thank all patients who participated in the study.

## Author contributions

JT: Conceptualization, Writing—Review and Editing, Project administration, Funding acquisition. XZ and ML: Investigation, Software, Validation, Formal analysis, Writing—Original Draft, Visualization. LS, YC, ST, GL, TL: Resources, Sample collection, and procession, Clinical data collation. YY, WX, and ZW: Data Curation, Supervision. All authors reviewed the manuscript and gave final approval of the submitted manuscript.

## Funding

This work was supported by Grants from the General Project of Natural Science Foundation of Hunan Province (No. 2020JJ4051); Promotion Project of Health Suitability Program in Health Department of Hunan Province (No. WZ2020-15); Science and Technology Innovation Program of Hunan Province (No. 2020SK51101); Hunan Cancer Hospital Climbing Fund (No. ZX2020004); Capacity Building Project of Central Subsidy Medical and Health Institutions (No. 20201127-1001); Key Specialty Construction Project in Hunan Province (No. 20210826-1004); General Project in Health Department of Hunan Province (No. 202205015388).

## Availability of data and materials

RNA sequence data of all samples were publically stored in the Gene Expression Omnibus of NCBI, GSE223126 (<https://www.ncbi.nlm.nih.gov/geo/query/acc.cgi?acc=GSE223126>). The accession numbers of previously published datasets involved in our study were GSE113486 [26], GSE94533 [27], and GSE61568 [22].

## Declarations

### Ethics approval and consent to participate

The study was obtained ethical approval (No. KYJJ-2019-043) from the Ethics Committee of Hunan Cancer Hospital / the Affiliated Tumor Hospital of Xiangya School of Medicine, Central South University. Written informed consent was provided by each participant before collecting samples.

### Consent for publication

Not applicable.

## Competing interests

The authors declare that they have no competing interests.

## Author details

<sup>1</sup>Department of Gynecologic Oncology, Hunan Cancer Hospital, The Affiliated Cancer Hospital of Xiangya School of Medicine, Central South University, Changsha 410013, People's Republic of China. <sup>2</sup>Department of Gynecology and Obstetrics, The Central Hospital of Shaoyang, Shaoyang 422000, People's Republic of China. <sup>3</sup>Department of Gynecology and Obstetrics, The First People's Hospital of Huaihua, The Affiliated Huaihua Hospital of University of South China, Huaihua 418000, People's Republic of China. <sup>4</sup>Department of Gynecology and Obstetrics, The First People's Hospital of Changde, Changde 415000, People's Republic of China. <sup>5</sup>Department of Gynecology and Obstetrics, The First People's Hospital of Yueyang, Yueyang 414000, People's Republic of China. <sup>6</sup>Department of Gynecologic Oncology, Hunan Gynecologic Cancer Research Center, Hunan Cancer Hospital, The Affiliated Cancer Hospital of Xiangya School of Medicine, Central South University, Address: 283 Tongzipo Road, Yuelu District, Changsha 410013, People's Republic of China. <sup>7</sup>Department of Oncology, Xiangya Cancer Center, Xiangya Hospital, Central South University, Changsha 410008, People's Republic of China.

Received: 8 June 2023 Accepted: 28 November 2023

Published online: 22 December 2023

## References

- Siegel RL, Miller KD, Fuchs HE, Jemal A. Cancer statistics. *CA Cancer J Clin.* 2021;71:7–33.
- Horowitz NS, Miller A, Rungruang B, Richard SD, Rodriguez N, Bookman MA, Hamilton CA, Krivak TC, Maxwell GL. Does aggressive surgery improve outcomes? Interaction between preoperative disease burden and complex surgery in patients with advanced-stage ovarian cancer: an analysis of gog 182. *J Clin Oncol.* 2015;33:937–43.
- William EW, Maxwell GL, Tian C, Sundborg MJ, Rose GS, Rose PG, Rubin SC, Muggia F, Mcguire WP, Gynecologic OG. Tumor residual after surgical cytoreduction in prediction of clinical outcome in stage iv epithelial ovarian cancer: a gynecologic oncology group study. *J Clin Oncol.* 2008;26:83–9.
- Vergote I, Coens C, Nankivell M, Kristensen GB, Parmar M, Ehlen T, Jayson GC, Johnson N, Swart AM, Verheijen R, Mccluggage WG, Perren T, Panici PB, Kenter G, Casado A, Mendiola C, Stuart G, Reed NS, Kehoe S. Neoadjuvant chemotherapy versus debulking surgery in advanced tubo-ovarian cancers: pooled analysis of individual patient data from the eortc 55971 and chorus trials. *Lancet Oncol.* 2018;19:1680–7.
- Suidan RS, Ramirez PT, Sarasohn DM, Teitcher JB, Iyer RB, Zhou Q, Iasonos A, Denesopolis J, Zivanovic O, Long Roche KC, Sonoda Y, Coleman RL, Abu-Rustum NR, Hricak H, Chi DS. A multicenter assessment of the ability of preoperative computed tomography scan and ca-125 to predict gross residual disease at primary debulking for advanced epithelial ovarian cancer. *Gynecol Oncol.* 2017;145:27–31.
- Suidan RS, Ramirez PT, Sarasohn DM, Teitcher JB, Mironov S, Iyer RB, Zhou Q, Iasonos A, Paul H, Hosaka M, Aghajanian CA, Leitao MJ, Gardner GJ, Abu-Rustum NR, Sonoda Y, Levine DA, Hricak H, Chi DS. A multicenter prospective trial evaluating the ability of preoperative computed tomography scan and serum ca-125 to predict suboptimal cytoreduction at primary debulking surgery for advanced ovarian, fallopian tube, and peritoneal cancer. *Gynecol Oncol.* 2014;134:455–61.
- Fagotti A, Ferrandina G, Fanfani F, Garganese G, Vizzielli G, Carone V, Salerno MG, Scambia G. Prospective validation of a laparoscopic predictive model for optimal cytoreduction in advanced ovarian carcinoma. *Am J Obstet Gynecol.* 2008;199:641–2.
- Vizzielli G, Costantini B, Tortorella L, Pitruzzella I, Gallotta V, Fanfani F, Gueli AS, Cosentino F, Nero C, Scambia G, Fagotti A. A laparoscopic risk-adjusted model to predict major complications after primary debulking surgery in ovarian cancer: a single-institution assessment. *Gynecol Oncol.* 2016;142:19–24.
- Brun JL, Rouzier R, Uzan S, Daraï E. External validation of a laparoscopic-based score to evaluate resectability of advanced ovarian cancers: clues for a simplified score. *Gynecol Oncol.* 2008;110:354–9.

10. Moller A, Lobb RJ. The evolving translational potential of small extracellular vesicles in cancer. *Nat Rev Cancer*. 2020;20:697–709.
11. Yang X, Su W, Chen X, Geng Q, Zhai J, Shan H, Guo C, Wang Z, Fu H, Jiang H, Lin J, Lagisetty KH, Zhang J, Li Y, Yang S, Massion PP, Beer DG, Chang AC, Ramnath N, Chen G. Validation of a serum 4-miRNA signature for the detection of lung cancer. *Transl Lung Cancer Res*. 2019;8:636–48.
12. Alhasan AH, Scott AW, Wu JJ, Feng G, Meeks JJ, Thaxton CS, Mirkin CA. Circulating miRNA signature for the diagnosis of very high-risk prostate cancer. *Proc Natl Acad Sci U S A*. 2016;113:10655–60.
13. Taylor DD, Gercel-Taylor C. MicroRNA signatures of tumor-derived exosomes as diagnostic biomarkers of ovarian cancer. *Gynecol Oncol*. 2008;110:13–21.
14. Yokoi A, Matsuzaki J, Yamamoto Y, Yoneoka Y, Takahashi K, Shimizu H, Uehara T, Ishikawa M, Ikeda S, Sonoda T, Kawauchi J, Takizawa S, Aoki Y, Niida S, Sakamoto H, Kato K, Kato T, Ochiya T. Integrated extracellular miRNA profiling for ovarian cancer screening. *Nat Commun*. 2018. <https://doi.org/10.1038/s41467-018-06434-4>.
15. Muller L, Hong CS, Stolz DB, Watkins SC, Whiteside TL. Isolation of biologically-active exosomes from human plasma. *J Immunol Methods*. 2014;411:55–65.
16. Théry C, Amigorena S, Raposo G, Clayton A. Isolation and characterization of exosomes from cell culture supernatants and biological fluids. *Curr Protoc Cell Biol*. 2006. <https://doi.org/10.1002/0471143030>.
17. Théry C, Witwer KW, Aikawa E, Alcaraz MJ, Anderson JD, Andriantsitohaina R, Antoniou A, et al. Minimal information for studies of extracellular vesicles 2018 (mivse2018): a position statement of the international society for extracellular vesicles and update of the mivse2014 guidelines. *J Extracellular Vesicles*. 2018;7:1535750.
18. Vella LJ, Scicluna BJ, Cheng L, Bawden EG, Masters CL, Ang CS, Williamson N, Mclean C, Barnham KJ, Hill AF. A rigorous method to enrich for exosomes from brain tissue. *J Extracell Vesicles*. 2017;6:1348885.
19. Crescitelli R, Lässer C, Lötvall J. Isolation and characterization of extracellular vesicle subpopulations from tissues. *Nat Protoc*. 2021;16:1548–80.
20. Li L, Li C, Wang S, Wang Z, Jiang J, Wang W, Li X, Chen J, Liu K, Li C, Zhu G. Exosomes derived from hypoxic oral squamous cell carcinoma cells deliver mir-21 to normoxic cells to elicit a prometastatic phenotype. *Cancer Res*. 2016;76:1770–80.
21. Jin N, Bi A, Lan X, Xu J, Wang X, Liu Y, Wang T, Tang S, Zeng H, Chen Z, Tan M, Ai J, Xie H, Zhang T, Liu D, Huang R, Song Y, Leung EL, Yao X, Ding J, Geng M, Lin SH, Huang M. Identification of metabolic vulnerabilities of receptor tyrosine kinases-driven cancer. *Nat Commun*. 2019;10:2701.
22. Tothill RW, Tinker AV, George J, Brown R, Fox SB, Lade S, Johnson DS, Trivett MK, Etemadmoghadam D, Locandro B, Traficante N, Fereday S, Hung JA, Chiew YE, Haviv I, Gertig D, Defazio A, Bowtell DDL. Novel molecular subtypes of serous and endometrioid ovarian cancer linked to clinical outcome. *Clin Cancer Res*. 2008;14:5198–208.
23. Wong LL, Zou R, Zhou L, Lim JY, Phua D, Liu C, Chong J, Ng J, Liew OW, Chan SP, Chen YT, Chan M, Yeo P, Ng TP, Ling LH, Sim D, Leong K, Ong HY, Jauffeerally F, Wong R, Chai P, Low AF, Lund M, Devlin G, Troughton R, Cameron VA, Doughty RN, Lam C, Too HP, Richards AM. Combining circulating miRNA and nt-probnp to detect and categorize heart failure subtypes. *J Am Coll Cardiol*. 2019;73:1300–13.
24. Nishiwada S, Sho M, Banwait JK, Yamamura K, Akahori T, Nakamura K, Baba H, Goel A. A miRNA signature identifies pancreatic ductal adenocarcinoma patients at risk for lymph node metastases. *Gastroenterology*. 2020;159:562–74.
25. Pencina MJ, D'Agostino RS, D'Agostino RJ, Vasan RS. Evaluating the added predictive ability of a new marker: from area under the roc curve to reclassification and beyond. *Stat Med*. 2008;27(157–172):207–12.
26. Usuba W, Urabe F, Yamamoto Y, Matsuzaki J, Sasaki M, Ichikawa M, Takizawa S, Aoki Y, Niida S, Kato K, Egawa S, Chikaraishi T, Fujimoto H, Ochiya T. Circulating miRNA panels for specific and early detection in bladder cancer. *Cancer Sci*. 2019;110:408–19.
27. Elias KM, Fendler W, Stawiski K, Fiascone SJ, Vitonis AF, Berkowitz RS, Frenkl G, Konstantinopoulos P, Crum CP, Kedzierska M, Cramer DW, Chowdhury D. Diagnostic potential for a serum miRNA neural network for detection of ovarian cancer. *Elife*. 2017. <https://doi.org/10.7554/eLife.28932>.
28. Network TCGA. Integrated genomic analyses of ovarian carcinoma. *Nature*. 2011;474:609–15.
29. Cohen JD, Li L, Wang Y, Thoburn C, Afsari B, Danilova L, et al. Detection and localization of surgically resectable cancers with a multi-analyte blood test. *Science*. 2018;359:926–30.
30. Bast RJ, Klug TL, St JE, Jenison E, Niloff JM, Lazarus H, Berkowitz RS, Leavitt T, Griffiths CT, Parker L, Zurawski VJ, Knapp RC. A radioimmunoassay using a monoclonal antibody to monitor the course of epithelial ovarian cancer. *N Engl J Med*. 1983;309:883–7.
31. So J, Kapoor R, Zhu F, Koh C, Zhou L, Zou R, et al. Development and validation of a serum miRNA biomarker panel for detecting gastric cancer in a high-risk population. *Gut*. 2021;70:829–37.
32. Yang Z, Lariviere MJ, Ko J, Till JE, Christensen T, Yee SS, et al. A multianalyte panel consisting of extracellular vesicle miRNAs and mRNAs, cfDNA, and ca19-9 shows utility for diagnosis and staging of pancreatic ductal adenocarcinoma. *Clin Cancer Res*. 2020;26:3248–58.
33. Ostensfeld MS, Jensen SG, Jeppesen DK, Christensen LL, Thorsen SB, Stenvang J, et al. MiRNA profiling of circulating epcam(+) extracellular vesicles: promising biomarkers of colorectal cancer. *J Extracell Vesicles*. 2016;5:31488.
34. Turner N, Grose R. Fibroblast growth factor signalling: from development to cancer. *Nat Rev Cancer*. 2010;10:116–29.
35. Albelda SM, Muller WA, Buck CA, Newman PJ. Molecular and cellular properties of pecam-1 (endocam/cd31): a novel vascular cell-cell adhesion molecule. *J Cell Biol*. 1991;114:1059–68.
36. Hermiston ML, Xu Z, Weiss A. Cd45: a critical regulator of signaling thresholds in immune cells. *Annu Rev Immunol*. 2003;21:107–37.
37. Nagrath S, Sequist LV, Maheswaran S, Bell DW, Irimia D, Ullkus L, Smith MR, Kwak EL, Digumarthy S, Muzikansky A, Ryan P, Balis UJ, Tompkins RG, Haber DA, Toner M. Isolation of rare circulating tumour cells in cancer patients by microchip technology. *Nature*. 2007;450:1235–9.
38. van der Pol E, Böing AN, Gool EL, Nieuwland R. Recent developments in the nomenclature, presence, isolation, detection and clinical impact of extracellular vesicles. *J Thromb Haemost*. 2016;14:48–56.
39. Jiang R, Zhu J, Kim JW, Liu J, Kato K, Kim HS, et al. Study of upfront surgery versus neoadjuvant chemotherapy followed by interval debulking surgery for patients with stage iiic and iv ovarian cancer, sgog sunny (soc-2) trial concept. *J Gynecol Oncol*. 2020;31: e86.
40. Grabowski JP, Harter P, Heitz F, Pujade-Lauraine E, Reuss A, Kristensen G, Ray-Coquard I, Heitz J, Traut A, Pfisterer J, du Bois A. Operability and chemotherapy responsiveness in advanced low-grade serous ovarian cancer: an analysis of the ago study group metadatabase. *Gynecol Oncol*. 2016;140:457–62.
41. Tucker SL, Gharpure K, Herbrich SM, Unruh AK, Nick AM, Crane EK, et al. Molecular biomarkers of residual disease after surgical debulking of high-grade serous ovarian cancer. *Clin Cancer Res*. 2014;20:3280–8.
42. Nakamura K, Sawada K, Yoshimura A, Kinose Y, Nakatsuka E, Kimura T. Clinical relevance of circulating cell-free miRNAs in ovarian cancer. *Mol Cancer*. 2016;15:48.
43. Benedetti PP, Di Donato V, Fischetti M, Casorelli A, Perniola G, Musella A, Marchetti C, Palaia I, Berloco P, Muzii L. Predictors of postoperative morbidity after cytoreduction for advanced ovarian cancer: analysis and management of complications in upper abdominal surgery. *Gynecol Oncol*. 2015;137:406–11.
44. O'Brien K, Breyné K, Ughetto S, Laurent LC, Breakefield XO. Rna delivery by extracellular vesicles in mammalian cells and its applications. *Nat Rev Mol Cell Biol*. 2020;21:585–606.
45. Wang W, Yang J, Xiang YY, Pi J, Bian J. Overexpression of hsa-mir-320 is associated with invasion and metastasis of ovarian cancer. *J Cell Biochem*. 2017;118:3654–61.
46. Lieb V, Weigelt K, Scheinost L, Fischer K, Greither T, Marcou M, Theil G, Klocker H, Holzhausen HJ, Lai X, Vera J, Kicic AB, Horninger W, Fornara P, Wullich B, Taubert H, Wach S. Serum levels of mir-320 family members are associated with clinical parameters and diagnosis in prostate cancer patients. *Oncotarget*. 2018;9:10402–16.
47. Wen Y, Han J, Chen J, Dong J, Xia Y, Liu J, Jiang Y, Dai J, Lu J, Jin G, Han J, Wei Q, Shen H, Sun B, Hu Z. Plasma miRNAs as early biomarkers for detecting hepatocellular carcinoma. *Int J Cancer*. 2015;137:1679–90.
48. Su YY, Sun L, Guo ZR, Li JC, Bai TT, Cai XX, Li WH, Zhu YF. Upregulated expression of serum exosomal mir-375 and mir-1307 enhance the diagnostic power of ca125 for ovarian cancer. *J Ovarian Res*. 2019;12:6.

49. Shimomura A, Shiino S, Kawauchi J, Takizawa S, Sakamoto H, Matsuzaki J, Ono M, Takeshita F, Niida S, Shimizu C, Fujiwara Y, Kinoshita T, Tamura K, Ochiya T. Novel combination of serum microRNA for detecting breast cancer in the early stage. *Cancer Sci.* 2016;107:326–34.
50. Ge L, Zhang N, Li D, Wu Y, Wang H, Wang J. Circulating exosomal small rnas are promising non-invasive diagnostic biomarkers for gastric cancer. *J Cell Mol Med.* 2020;24:14502–13.
51. Ali S, Almhanna K, Chen W, Philip PA, Sarkar FH. Differentially expressed mirnas in the plasma may provide a molecular signature for aggressive pancreatic cancer. *Am J Transl Res.* 2010;3:28–47.
52. Aly DM, Gohar NA, Abd EA, Khairy M, Abdullatif MM. Serum microRNA let-7a-1/let-7d/let-7f and mirna 143/145 gene expression profiles as potential biomarkers in hcv induced hepatocellular carcinoma. *Asian Pac J Cancer Prev.* 2020;21:555–62.
53. Zheng M, Hou L, Ma Y, Zhou L, Wang F, Cheng B, Wang W, Lu B, Liu P, Lu W, Lu Y. Exosomal let-7d-3p and mir-30d-5p as diagnostic biomarkers for non-invasive screening of cervical cancer and its precursors. *Mol Cancer.* 2019. <https://doi.org/10.1186/s12943-019-0999-x>.
54. Buamah P. Benign conditions associated with raised serum ca-125 concentration. *J Surg Oncol.* 2000;75:264–5.
55. Min L, Zhu S, Chen L, Liu X, Wei R, Zhao L, Yang Y, Zhang Z, Kong G, Li P, Zhang S. Evaluation of circulating small extracellular vesicles derived mirnas as biomarkers of early colon cancer: a comparison with plasma total mirnas. *J Extracell Vesicles.* 2019;8:1643670.

### Publisher's Note

Springer Nature remains neutral with regard to jurisdictional claims in published maps and institutional affiliations.

Ready to submit your research? Choose BMC and benefit from:

- fast, convenient online submission
- thorough peer review by experienced researchers in your field
- rapid publication on acceptance
- support for research data, including large and complex data types
- gold Open Access which fosters wider collaboration and increased citations
- maximum visibility for your research: over 100M website views per year

At BMC, research is always in progress.

Learn more [biomedcentral.com/submissions](https://biomedcentral.com/submissions)

